

# Disordered solid to Bose-glass transition in Bose-Hubbard model with disorder and long-range interactions

Kohenjit Pebam, Laxmi Angom, Bhumika Thoudam, Momin Hrangbung, Deepak Gaur and Dilip Angom  
*Manipur University, Canchipur-795003, Physics Department*

The introduction of disorder in Bose-Hubbard model gives rise to new glassy quantum phases, namely the Bose-glass (BG) and disordered solid (DS) phases. In this work, we present the rich phase diagram of interacting bosons in disordered two-dimensional optical lattice, modelled by the disordered Bose-Hubbard model. We systematically probe the effect of long-range interaction truncated to the nearest neighbors and next-nearest neighbors on the phase diagram. We investigate the zero-temperature ground-state quantum phases using the single-site Gutzwiller mean field (SGMF) theory. We also employ strong-coupling perturbative expansion to identify the nature of ground-state solid phases analytically. At sufficiently high disorder strength, we observe a quantum phase transition between the DS and BG phases. We have investigated this transition in greater detail using cluster Gutzwiller mean field theory to study the effect of inter-site correlations which is absent in the SGMF method. We have also studied this phase transition from the perspective of percolation theory.

## I. INTRODUCTION

The disordered systems have been a subject of several studies and continues to attract attention. This is primarily fueled by its intimate connections with the real-world physical systems. These systems are characterized by deviations from long-range ordering, which may be attributed to the randomness in some of the components in the system. The disordered quantum systems have attracted significant attention and the studies on these systems have led to the discovery of fascinating phenomena such as Anderson localization [1, 2] and the glassy quantum phases such as Bose-glass [3, 4], to name a few. Disordered quantum many-body systems of interacting bosons have been explored in various experiments and theoretical studies [4–12]. In the theoretical studies, these systems are modelled using the disordered Bose-Hubbard model (DBHM) [3] which is experimentally realizable with optical lattices and speckle laser fields [13, 14] for creating the random disorder in the lattice potential. In recent years, ultracold atoms in optical lattices have emerged as an ideal platform to simulate the physics of quantum many-body systems. This is due to the developments of novel experimental techniques to manipulate the system parameters together with the accessibility of the strongly interacting regime [15–19]. Such a system of bosonic atoms is modelled by the Bose-Hubbard model (BHM) and its extensions [3, 20].

The BHM exhibits a metal-insulator transition between superfluid (SF) and Mott insulator (MI) quantum phases which have been observed in experiments with optical lattices [21]. In the DBHM, for any strength of disorder, the BG phase intervenes the metal-insulator transition in the thermodynamic limit [22]. The effects of long-range interactions can be probed in BHM by using dipolar atoms, molecules or Rydberg atoms in optical lattices, and the modified system is then referred to as the extended BHM. These interactions introduce a new quantum phase referred as the supersolid (SS) phase which have both the superfluid property as well as crystalline order [23–27]. This novel phase has been recently observed in the experiments [28–31]. The introduction of disorder leads to emergence of other novel quantum phases called disordered solid and BG phase. In this work, we report the

rich phase diagram of the disordered extended Bose-Hubbard model (DEBHM). We have studied the effect of dipolar interactions, beyond the standard truncation to nearest neighbors (NN) only [9], and have studied the effect of next-nearest neighbors (NNN) on the phase diagram. This gives a richer phase diagram with insulating phases having average occupancies  $\rho = 1/4$  and  $\rho = 3/4$ , which is absent in the NN truncation.

In the present work, we employ the SGMF theory [32, 33] to study the ground-state quantum phases of softcore dipolar bosons in  $2D$  square optical lattices. The DEBHM exhibits a rich phase diagram comprising of six types of quantum phases, namely the MI, density wave (DW), DS, BG, SS and SF phases at zero temperature and are demarcated by various quantum phase transitions. Using strong coupling perturbative expansion, we also examine the nature of the insulating ground state among the checkerboard and stripe geometry for density wave phases and the results agree with the numerical results obtained using SGMF method. Earlier works had reported the transition from DS to BG in the hardcore limit [34]. Our results using SGMF method, shows this phase transition for the case of softcore bosons, which we study in better detail by accounting the effect of quantum correlations using the cluster Gutzwiller mean-field (CGMF) theory [35]. The compressibility and structure factor calculations are also done using CGMF and comparison is made with the results obtained using SGMF. The CGMF results suggests an enlargement of the BG phase domain whereas domain of DS phase shrinks. The other approach to characterize the DS and BG phases is to focus on the background phase. In short, DS phase has a structured background whereas it is uniform in BG phase. Considering this we analyze the DS-BG phase transition from the viewpoint of the percolation transition and investigate the critical value of chemical potential when the spanning cluster emerges in the systems. It is to be mentioned that the concepts and tools from percolation theory have wide applicability across various types of systems [36–39]. The paper is organized as follows. In Sec. II, we introduce the model Hamiltonian and provide a description of the SGMF method used to obtain the zero temperature ground-state phase diagrams in our study. The various order parameters employed

to differentiate the quantum phases from each other are also described here. Sec. III presents the strong-coupling perturbative expansion results involving comparison of the density wave phases to identify the structure of the ground-state solid quantum phases. In Sec. IV, we present the ground state phase diagrams of DEBHM at different disorder strengths, for the cases involving truncation of dipolar interactions till NN and NNN sites. Here, we also discuss on the DS-BG phase transition. Finally, Sec. V presents the conclusion of our work.

## II. THEORETICAL METHODS

A system of ultracold bosons with long-range interaction and disorder in a square optical lattice is well described by the DEBHM. The Hamiltonian of the system is

$$\begin{aligned} \hat{H}_{\text{DEBHM}} = & - \sum_{p,q} \left( J_x \hat{b}_{p+1,q}^\dagger \hat{b}_{p,q} + J_y \hat{b}_{p,q+1}^\dagger \hat{b}_{p,q} + \text{H.c.} \right) \\ & + \sum_{p,q} \hat{n}_{p,q} \left[ \frac{U}{2} (\hat{n}_{p,q} - 1) - \tilde{\mu}_{p,q} \right] \\ & + \sum_{\xi,\xi'} \frac{V_{\xi,\xi'}}{2} \hat{n}_\xi \hat{n}_{\xi'}, \end{aligned} \quad (1)$$

where  $p(q)$  is the lattice site index along the  $x(y)$  direction,  $\hat{b}_{p,q}^\dagger (\hat{b}_{p,q})$  is the boson creation (annihilation) operator at the lattice site  $(p, q)$ ,  $\hat{n}_{p,q} = \hat{b}_{p,q}^\dagger \hat{b}_{p,q}$  is the number operator for bosons,  $J_x$  and  $J_y$  are the tunneling strength along the  $x$  and  $y$  directions respectively. The effective chemical potential  $\tilde{\mu}_{p,q} = \mu - \epsilon_{p,q}$  consist of the average chemical potential  $\mu$  and the disorder  $\epsilon_{p,q}$ . The disorder is a random energy offset introduced using random numbers distributed uniformly with  $\epsilon_{p,q} \in [-D, D]$  and  $D$  is the bound of random numbers. The on-site interaction energy is  $U > 0$ . For compact notations,  $\xi \equiv (p, q)$  and  $\xi' \equiv (p', q')$  represent the lattice indices of the neighbouring sites. To represent the long range potential we consider the  $V_1 - V_2$  model [26], which has the expression

$$V_{\xi,\xi'} = \begin{cases} V_1 & \text{if } |\mathbf{r}_\xi - \mathbf{r}_{\xi'}| = a, \\ V_2 & \text{if } |\mathbf{r}_\xi - \mathbf{r}_{\xi'}| = \sqrt{2}a, \\ 0 & \text{otherwise,} \end{cases} \quad (2)$$

where  $a$  is the lattice constant and  $\mathbf{r}_\xi$  and  $\mathbf{r}_{\xi'}$  are the position vectors of the  $\xi$  and  $\xi'$  lattice sites, respectively.  $V_1 \geq 0$  and  $V_2 \geq 0$  are the nearest neighbour (NN) and next nearest neighbour (NNN) interactions. Here,  $V_1$  and  $V_2$  are related through the relation  $V_2/V_1 = 1/(2\sqrt{2})$ . This relation corresponds to the inverse cube power law of the isotropic dipole-dipole interaction.

### A. Single-site Gutzwiller mean-field (SGMF) theory

The SGMF theory is a mean-field theory employed to study the ground state of the lattices like the case of disordered extended Bose-Hubbard model which is described by Eq.(1). In

the SGMF theory, the bosonic operators are approximated as sum of their expectation values and quantum fluctuations

$$\begin{aligned} \hat{b}_\xi &= \phi_\xi + \delta \hat{b}_\xi, \\ \hat{b}_\xi^\dagger &= \phi_\xi^* + \delta \hat{b}_\xi^\dagger. \end{aligned} \quad (3)$$

Then the product of the creation and the annihilation operators can be written as

$$\hat{b}_\xi^\dagger \hat{b}_{\xi'} \approx \phi_\xi^* \phi_{\xi'} + \hat{b}_\xi^\dagger \phi_{\xi'} - \phi_\xi^* \phi_{\xi'}. \quad (4)$$

Here,  $\phi_\xi = \langle \hat{b}_\xi \rangle$  is the SF order parameter at the lattice site  $\xi$ . Similarly, like earlier, to find the mean field approximation of the long range part, we expand  $\hat{n}_\xi$  and  $\hat{n}_{\xi'}$  as the sum of their expectation values and quantum fluctuations

$$\begin{aligned} \hat{n}_\xi &= \langle \hat{n}_\xi \rangle + \delta \hat{n}_\xi, \\ \hat{n}_{\xi'} &= \langle \hat{n}_{\xi'} \rangle + \delta \hat{n}_{\xi'}. \end{aligned}$$

Neglecting the fluctuations, the density dependence in the long-range interaction can be written as

$$\hat{n}_\xi \hat{n}_{\xi'} \approx \hat{n}_\xi \langle \hat{n}_{\xi'} \rangle + \langle \hat{n}_\xi \rangle \hat{n}_{\xi'} - \langle \hat{n}_\xi \rangle \langle \hat{n}_{\xi'} \rangle. \quad (5)$$

Using the above approximations, the single-site mean-field Hamiltonian of the system is

$$\begin{aligned} \hat{H}_{p,q}^{\text{MF}} = & - \left[ J_x \left( \phi_{p+1,q}^* \hat{b}_{p,q} - \phi_{p+1,q} \phi_{p,q} \right) \right. \\ & + J_y \left( \phi_{p,q+1}^* \hat{b}_{p,q} - \phi_{p,q+1} \phi_{p,q} \right) + \text{H.c.} \left. \right] \\ & + \hat{n}_{p,q} \left[ \frac{U}{2} (\hat{n}_{p,q} - 1) - \tilde{\mu}_{p,q} \right] \\ & + \sum_{\xi'} V_{\xi,\xi'} (\hat{n}_\xi \langle \hat{n}_{\xi'} \rangle - \langle \hat{n}_\xi \rangle \langle \hat{n}_{\xi'} \rangle), \end{aligned} \quad (6)$$

The mean-field Hamiltonian of the system can be written as the sum of the single-site mean-field hamiltonians

$$\hat{H}_{\text{MF}} = \sum_{p,q} \hat{H}_{p,q}^{\text{MF}}. \quad (7)$$

With this approximation, the neighbouring lattice sites are coupled through the SF order parameter and the eigenstate of a single-site is a linear combination of the Fock states. Accordingly, the eigenstate of the whole system is the direct product of the single-site states. Thus, with the Gutzwiller ansatz, the many-body wave function of the ground state is

$$|\Psi\rangle = \prod_{p,q} |\psi\rangle_{p,q} = \prod_{p,q} \left( \sum_{n=0}^{N_b-1} c_n^{(p,q)} |n\rangle_{p,q} \right), \quad (8)$$

where  $|\psi\rangle_{p,q}$  is the single site ground state,  $N_b$  is the dimension of the Fock space,  $|n\rangle_{p,q}$  is the Fock state of  $n$  bosons occupying site  $(p, q)$ , and  $c_n^{(p,q)}$  are the coefficients of the linear combination. The normalization condition of the wave function is  $\sum_n |c_n^{(p,q)}|^2 = 1$ . The SF order parameter at a lattice site can be calculated as

$$\phi_{p,q} = \langle \Psi | \hat{b}_{p,q} | \Psi \rangle = \sum_{n=0}^{N_b-1} \sqrt{n} c_{n-1}^{(p,q)*} c_n^{(p,q)}. \quad (9)$$

However, as a measure of global system properties we use the system size averaged  $\phi$  which is defined as

$$\phi = \frac{\sum_{p,q} |\phi_{p,q}|}{N}, \quad (10)$$

where  $N$  is the total number of lattice sites in the system. Similarly, we define the disordered averaged SF order parameter

$$\Phi = \frac{1}{N_d} \sum_{i=1}^{N_d} \phi_i, \quad (11)$$

where,  $N_d$  is the number of disorder samples and  $\phi_i$  is the system size averaged SF order parameter of the  $i$ th sample. Similarly, the lattice site occupancy is

$$n_{p,q} = \langle \Psi | \hat{b}_{p,q}^\dagger \hat{b}_{p,q} | \Psi \rangle = \sum_{n=0}^{N_b-1} n |c_n^{(p,q)}|^2. \quad (12)$$

The quantities  $\phi$  and  $n_{p,q}$  are used to identify the quantum phases of the system. Our previous works [40, 41] may be referred for additional details on the single-site Gutzwiller mean-field method we have used in the present study.

### B. Characterization of phases

The ground state of DEBHM can be of different quantum phases depending on the parameters of the system. And, the quantum phases can be distinguished using order parameters which are measure of different properties. In the present work, we use superfluid fraction  $f_s$ ,  $\phi$ , structure factor  $S(\vec{q})$  and compressibility  $\kappa$ . For a quantum phase which is phase coherent like the SF, a finite energy is required to destroy the phase coherence. This implies that the SF phase acquires stiffness towards phase change or has phase rigidity. For the calculation of  $f_s$ , a twisted boundary condition(TBC) is imposed on the state such that when it is applied along  $x$  direction, the hopping term at the boundary is transformed as

$$J_x \left( \hat{b}_{p+1,q}^\dagger \hat{b}_{p,q} \right) \rightarrow J_x \left( \hat{b}_{p+1,q}^\dagger \hat{b}_{p,q} e^{i2\pi\varphi} \right), \quad (13)$$

where  $\varphi$  is the twist applied to hopping at the boundary the periodic boundary condition,  $L$  is the lattice size along  $x$  direction and  $i2\pi\varphi$  is the phase shift possessed by an atom when it tunnels between the nearest neighbour lattice sites. With the introduction of TBC, the DEBHM Hamiltonian is modified and let the corresponding groundstate energy be  $E_\varphi$ . Let  $E_0$  be the energy eigenvalue corresponding to DEBHM Hamiltonian without TBC. Then superfluid fraction  $f_s$ , expressed in terms of the DEBHM Hamiltonian parameters, is given as [42]

$$f_s = \frac{I^2}{NJ\varphi^2} [E_\varphi - E_0], \quad (14)$$

where  $I$  is the total lattice sites along a direction and  $N$  is the total occupancy of the system. Among the ground state quantum phases, MI and DW are incompressible and the remaining

quantum phases DS, BG, SS and SF are compressible. The compressibility of the system is defined using the following relation

$$\kappa = \frac{\partial \langle \hat{n} \rangle}{\partial \mu}. \quad (15)$$

The occupancies in the DW phase is a combination of two sublattices A and B with different fillings. This description implies that in the above equation  $\langle \hat{n}_\xi \rangle \equiv \langle \hat{n}_A \rangle$  and  $\langle \hat{n}_{\xi'} \rangle \equiv \langle \hat{n}_B \rangle$  are the sublattice occupancies of the two sublattices. Another order parameter which we used to determine the diagonal long-range order, characteristic of a solid or structured phase, is the structure factor  $S(\vec{q})$ . It is defined in terms of the density-density correlation function

$$S(\vec{q}) = \frac{1}{N} \sum_{\xi, \xi'} e^{i\vec{q} \cdot (\vec{r}_\xi - \vec{r}_{\xi'})} \langle \hat{n}_\xi \hat{n}_{\xi'} \rangle. \quad (16)$$

As an example consider the checkerboard density wave phase. One of its distinguishing property is a peak of  $S(\vec{q})$  at the wave vector  $\vec{q} = (\pi, \pi)$ . The order parameters employed to distinguish various quantum phases exhibited by DEBHM are listed in Table I.

TABLE I. Table showing values of different order parameters of different quantum phases exhibited by DEBHM.

Quantum phases	$ f_s $	$ S(\pi, \pi) $	$\phi$
$\frac{1}{4}$ DW	0	$\neq 0$ (integer)	0
CDW	0	$\neq 0$ (integer)	0
$\frac{3}{4}$ DW	0	$\neq 0$ (real)	0
SS	$\neq 0$	$\neq 0$ (real)	$\neq 0$
SF	$\neq 0$	=0	$\neq 0$
BG	=0	=0	$\neq 0$
DS	=0	$\neq 0$ (real)	$\neq 0$
MI	=0	=0	=0

### III. STRONG-COUPPLING PERTURBATIVE EXPANSION

To identify the quantum phase of the ground state analytically we use strong-coupling perturbation theory and apply it to the extended Bose-Hubbard model with both NN and NNN long-range interactions [43]. In the perturbative calculations we consider the insulating phases CDW and SDW unperturbed state. To identify the quantum phases of the system, we consider the system size as a  $4 \times 4$  square lattice. In this approach, the tunneling term in the extended Bose-Hubbard Hamiltonian is considered as the perturbation and

the remaining terms as the unperturbed Hamiltonian [43–45]. We, then, apply the many-body version of time-independent perturbation theory and expand the energy of the insulating phases in the powers of the tunneling parameter  $J$ . Due to the constraints on the choice of the unperturbed state, the method cannot be used to determine the phase boundary between two compressible phases. Using the method the perturbative expansion is calculated upto second order[46] for the CDW without extra particle as well as for SDW without extra particle. The extended Bose-Hubbard Hamiltonian is given by

$$\begin{aligned}\hat{H}_{\text{eBHM}} &= -J \sum_{\langle \xi, \xi' \rangle} (\hat{b}_{\xi}^{\dagger} \hat{b}_{\xi'} + \hat{b}_{\xi'}^{\dagger} \hat{b}_{\xi}) + \sum_{\xi} \left[ \frac{U}{2} \hat{n}_{\xi} (\hat{n}_{\xi} - 1) \right. \\ &\quad \left. - \mu \hat{n}_{\xi} \right] + \sum_{\xi, \xi'} \frac{V_{\xi \xi'}}{2} \hat{n}_{\xi} \hat{n}_{\xi'} \\ &= \hat{H}' + \hat{H}_0.\end{aligned}\quad (17)$$

In the Hamiltonian given above,  $H' = -J \sum_{\langle \xi, \xi' \rangle} (\hat{b}_{\xi}^{\dagger} \hat{b}_{\xi'} + \hat{b}_{\xi'}^{\dagger} \hat{b}_{\xi})$  is the perturbation term of the Hamiltonian and the remaining terms are the unperturbed terms  $\hat{H}_0$  [43, 44].

#### A. Ground-state wave functions of the insulating phases

With long-range interactions, DW phase can emerge as the ground state in certain parameter regimes since it lowers the repulsion between neighboring lattice sites. For the  $V_1 - V_2$  [26] model given by Eq. (2) with  $V_1 > 0$  and  $V_2 = 0$ , the checkerboard ordering lowers the repulsion between NN sites, resulting in the CDW phase as the ground state. Considering  $V_1 = 0$  and  $V_2 > 0$ , the stripe ordering is preferred as it lowers the repulsion between NNN sites can result in a lower energy. For intermediate values of  $V_1$  and  $V_2$ , the CDW and SDW phases needs to be compared for lower energy. In the SGMF theory, the generic form of the ground-state wave functions of the CDW and SDW phases is [43]

$$|\Psi_{\text{DW}}^{(0)}\rangle = \prod_{\xi \in A, \xi' \in B} |n_A\rangle_{\xi} |n_B\rangle_{\xi'}, \quad (18)$$

where,  $n_A$  and  $n_B$  as mentioned earlier are the occupancies at the lattice sites of sublattice  $A$  and  $B$ , respectively. More specifically, for the case of CDW phase the site indices  $\xi$  and  $\xi'$  satisfy the following conditions

$$\begin{aligned}\xi &\equiv (p, q) : p + q \text{ is even,} \\ \xi' &\equiv (p', q') : p' + q' \text{ is odd.}\end{aligned}\quad (19)$$

while for SDW phase similar relations, with stripes running along the  $y$ -axis, are

$$\begin{aligned}\xi &\equiv (p, q) : p \text{ is even,} \\ \xi' &\equiv (p', q') : p' \text{ is odd.}\end{aligned}\quad (20)$$

Other structured solid phases emerge when other terms in the long-range interactions are considered [24]. However, considering NN and NNN interactions we can probe the key features associated with combined effects of long-range interactions and disorder.

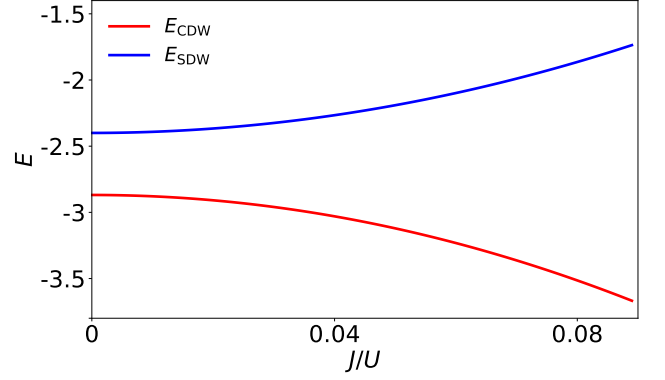


FIG. 1. Energy versus  $J$  plot showing comparison of  $E_{\text{CDW}}$  and  $E_{\text{SDW}}$  at  $\mu = 0.5$ ,  $V_1/U = 0.2$  and  $V_2/U = 0.0707$ . The blue curve is  $E_{\text{SDW}}$  and the red curve is for  $E_{\text{CDW}}$ . Here,  $E_{\text{CDW}}$  is found to be of lower energy compared to  $E_{\text{SDW}}$ .

#### B. Ground-state energies upto second order in $J$

In the strong-coupling perturbation expansion, we use the many-body version of the Rayleigh-Schrodinger perturbation theory. The perturbative expansion, as mentioned earlier, is in orders of  $J$  with respect to the ground state of the system. From the perturbation theory, the first order correction to the ground state energy is [43]

$$E_{\text{DW}}^{(1)} = \langle \Psi_{\text{DW}}^{(0)} | \hat{H}_0 | \Psi_{\text{DW}}^{(0)} \rangle. \quad (21)$$

Similarly, the second order correction to the ground state energy is given by the expression[46]

$$E_{\text{DW}}^{(2)} = \sum_{\Psi^{(\text{ex})} \neq \Psi_{\text{DW}}^{(0)}} \frac{\langle \Psi_{\text{DW}}^{(0)} | \hat{H}' | \Psi^{(\text{ex})} \rangle \langle \Psi^{(\text{ex})} | \hat{H}' | \Psi_{\text{DW}}^{(0)} \rangle}{(E_{\text{DW}}^{(0)} - E)}, \quad (22)$$

where  $|\Psi^{(\text{ex})}\rangle$  are excited states occurring as an intermediate state in the perturbation expansion. These are also the resulting states from the perturbation  $\hat{H}'$  operating on the ground state  $|\Psi_{\text{DW}}^{(0)}\rangle$  and  $E$  is the energy of the intermediate excited state  $|\Psi^{(\text{ex})}\rangle$ . We can, thus, define an intermediate excited state as

$$|\Psi^{(\text{ex})}\rangle = \frac{\hat{b}_{\xi}^{\dagger} \hat{b}_{\xi'}}{\sqrt{(n_{\xi} + 1)n_{\xi'}}} |\Psi_{\text{DW}}^{(0)}\rangle, \quad (23)$$

where,  $\xi$  and  $\xi'$  are the nearest neighbour lattice sites. Depending on the occupancies arising from different nearest-neighbour hopping, the CDW and SDW phases have two and four types of excited states, respectively. Thus, the intermedi-

ate excited states arising from the CDW phase are

$$\begin{aligned}
 |\Psi^{(\text{ex})}\rangle_{A-B+} &= |n_A - 1\rangle_\eta |n_B + 1\rangle_{\eta'} \prod_{\substack{\xi \in A, \xi' \in B \\ \xi \neq \eta, \xi' \neq \eta'}} |n_A\rangle_\xi |n_B\rangle_{\xi'}, \\
 |\Psi^{(\text{ex})}\rangle_{A+B-} &= |n_A + 1\rangle_\eta |n_B - 1\rangle_{\eta'} \prod_{\substack{\xi \in A, \xi' \in B \\ \xi \neq \eta, \xi' \neq \eta'}} |n_A\rangle_\xi |n_B\rangle_{\xi'}.
 \end{aligned} \tag{24}$$

Here, the subscripts  $A^+(A^-)$  denotes state with an addition (removal) of a boson at a site belonging to sublattice A. Similarly, the intermediate excited states of the SDW phase are

$$\begin{aligned}
 |\Psi^{(\text{ex})}\rangle_{A+B-} &= |n_A + 1\rangle_\eta |n_B - 1\rangle_{\eta'} \prod_{\substack{\xi \in A, \xi' \in B \\ \xi \neq \eta, \xi' \neq \eta'}} |n_A\rangle_\xi |n_B\rangle_{\xi'}, \\
 |\Psi^{(\text{ex})}\rangle_{B-B+} &= |n_B - 1\rangle_\eta |n_B + 1\rangle_{\eta'} \prod_{\substack{\xi \in A, \xi' \in B \\ \xi' \neq \eta, \eta'}} |n_A\rangle_\xi |n_B\rangle_{\xi'}, \\
 |\Psi^{(\text{ex})}\rangle_{A-B+} &= |n_A - 1\rangle_\eta |n_B + 1\rangle_{\eta'} \prod_{\substack{\xi \in A, \xi' \in B \\ \xi \neq \eta, \xi' \neq \eta'}} |n_A\rangle_\xi |n_B\rangle_{\xi'}, \\
 |\Psi^{(\text{ex})}\rangle_{A-A+} &= |n_A - 1\rangle_\eta |n_A + 1\rangle_{\eta'} \prod_{\substack{\xi \in A, \xi' \in B \\ \xi \neq \eta, \eta'}} |n_A\rangle_\xi |n_B\rangle_{\xi'}.
 \end{aligned} \tag{25}$$

In the above expressions,  $\eta$  and  $\eta'$  are the lattice sites where addition and removal of boson occurs respectively. The energies of CDW phase and SDW phase are calculated using the non-degenerate perturbation theory. These are given as

$$\begin{aligned}
 E_{\text{CDW}} &= \left[ \frac{8}{2} n_A (n_A - 1) U + \frac{8}{2} n_B (n_B - 1) U - 8\mu (n_A + n_B) \right. \\
 &\quad \left. + 32 n_A n_B V_1 + 16 n_A^2 V_2 + 16 n_B^2 V_2 \right] \\
 &\quad + \frac{32 n_A (n_B + 1) J^2}{(n_A - n_B - 1) U + V_1 + 4(n_A - n_B)(V_2 - V_1)} \\
 &\quad + \frac{32 n_B (n_A + 1) J^2}{(n_B - n_A - 1) U + V_1 + 4(n_B - n_A)(V_2 - V_1)}
 \end{aligned} \tag{26}$$

$$\begin{aligned}
 E_{\text{SDW}} &= \left[ \frac{8}{2} n_A (n_A - 1) U + \frac{8}{2} n_B (n_B - 1) U - 8\mu (n_A + n_B) \right. \\
 &\quad \left. + 8 n_A^2 V_1 + 8 n_B^2 V_1 + 16 n_A n_B V_1 + 32 n_A n_B V_2 \right] \\
 &\quad + \frac{16 n_B (n_A + 1) J^2}{(n_B - n_A - 1) U + V_1 + (n_A - n_B) V_2} \\
 &\quad + \frac{16 n_A (n_B + 1) J^2}{(n_A - n_B - 1) U + V_1 + (n_B - n_A) V_2} \\
 &\quad + \frac{16 n_B (n_B + 1) J^2 + 16 n_A (n_A + 1) J^2}{-U + V_1}.
 \end{aligned} \tag{27}$$

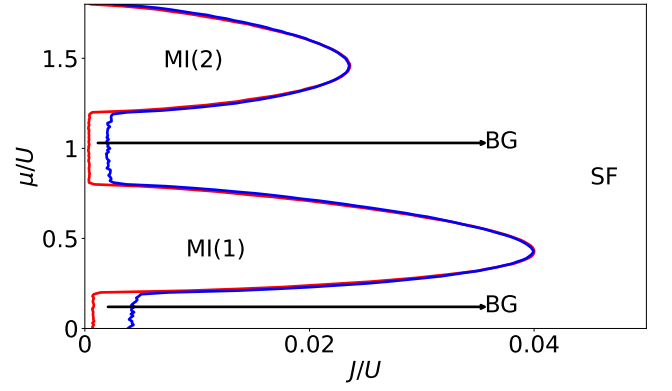


FIG. 2. Ground state phase diagram of DBHM at disorder strength  $D/U = 0.2$ . The red and blue phase boundaries indicates the MI-BG and BG-SF phase boundaries respectively.

## IV. RESULTS AND DISCUSSIONS

### A. Insulating ground states

The ground state of the system defined by the Hamiltonian in Eq. (1), for the case of  $J/U \approx 0$ , can be analytically identified using the method of strong coupling perturbative expansion. As discussed earlier the system supports two possible solid phases the CDW and SDW. The phase with the lower energy determines the ground state of the system. Consider the case of  $n_A = 1$  and  $n_B = 0$ , and considering that  $V_1/V_2 = 2\sqrt{2}$  the energies of the two phases given by Eqs. (26) and (27) are simplified to

$$E_{\text{CDW}} = -8\mu + 5.65V_1 - 20.17 \frac{J^2}{V_1}, \tag{28}$$

$$E_{\text{SDW}} = -8\mu + 8V_1 + 24.75 \frac{J^2}{V_1} + \frac{32J^2}{-1 + V_1}. \tag{29}$$

To compare the energies of the two states given above, we first compare the zeroth order energies. We express the long-range interaction terms in terms of  $V_1$  in both the expressions and we find that  $\frac{8}{\sqrt{2}}V_1 < 8V_1$ . This shows that zeroth order energy of (28) is lower than zeroth order energy of (29). Thus, at the zeroth order, the CDW is the favoured state. Next, let us compare the second order energy correction between the two expressions after scaling all the long-range interaction terms with  $V_1$ . In this case too, the CDW has lower energy. The trend of the energies corresponding to the CDW and SDW phases obtained from Eqs. (28) and (29) are shown in Fig. 1. From the figure it is evident that CDW has lower energy for all values of  $J/U$ . Thus, with the dipolar form of isotropic interaction CDW is the favoured ground state. This is along the expected lines as the NN interaction favours CDW, and with the dipolar form of long-range interaction the NNN interaction cannot lower the energy of the SDW to emerge as the ground state.



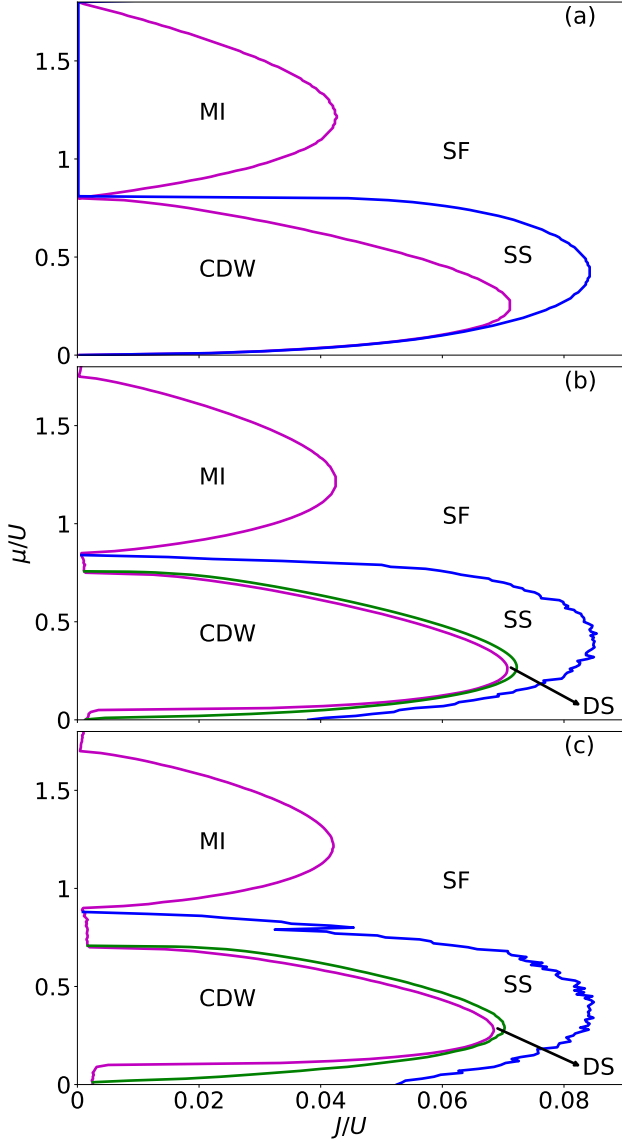


FIG. 3. Ground state phase diagram of DEBHM for  $V_1/U = 0.2$  and  $D/U = 0$  (a), 0.05 (b) and 0.1 (c). With non-zero disorder, the DS phase appears in the phase diagram, forming an envelope around the CDW phase.

### B. Phase diagram from SGMF

To calculate the ground state with SGMF, the parameters in the DEBHM Hamiltonian are scaled with respect to the on-site interaction energy  $U$ . Thus the relevant parameters are  $J/U$ ,  $\mu/U$ ,  $D/U$ ,  $V_1/U$  and  $V_2/U$ . For the present work, we consider a system size of  $50 \times 50$ . This implies that the system consists of 2500 lattice sites and this is large enough to provide reliable statistics. To introduce disorder, each lattice site is assigned a random number from a univariate distribution within the bound  $[-D, D]$ . As mentioned earlier, the disorder combines with the chemical potential and yields the effective chemical potential of a lattice site. One difficulty associated

with disordered systems is, one has to do a disorder averaging by repeating the calculations with different disorder realizations. To obtain reliable average properties the averaging must be done over a large number of samples. This requirement is to be balanced with the computational cost of considering a large system size. For the mean-field calculation the dimension of the Fock space is  $N_b = 5$ . And, the disorder averaging of the order parameters and properties are done over 50 disorder samples.

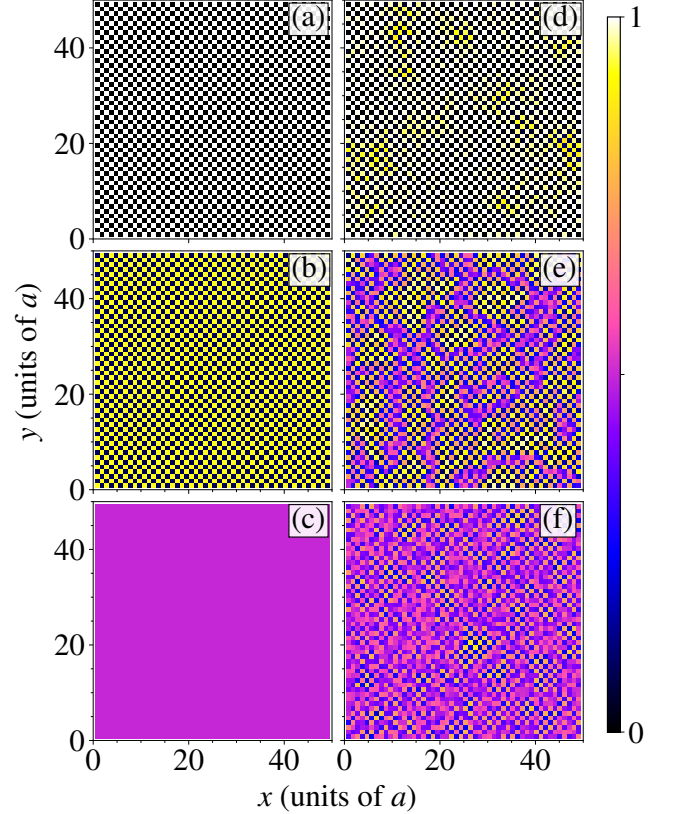


FIG. 4. Distribution of bosons on a  $50 \times 50$  lattice for  $\mu/U=0.29$  and  $V_1/U=0.2$ . Panels (a), (b) and (c) shows the CDW, SS and SF phases at  $J/U = 0.07, 0.075$  and  $0.087$  respectively, with  $D/U = 0$ . Panels (d), (e) and (f) shows the DS, SS and SF phases with the disorder strength  $D/U = 0.1$  for  $J/U = 0.07, 0.075$  and  $0.087$  respectively.

After identifying the ground state quantum phases, we generate the phase diagram in the  $J/U - \mu/U$ -plane by selecting a suitable order parameter to demarcate the phase boundaries. Using the order parameter, for a specific value of  $\mu/U$ , we employ bisection method along  $J/U$  to locate the critical point between two neighbouring quantum phases. In the case of incompressible-compressible phase boundary we use the system size averaged SF order parameter  $\phi$  as the order parameter and threshold of  $\phi \leq 10^{-4}$  in the bisection method. In the phase diagram, the DW lobes are enveloped by DS, and the DW-DS transition is of incompressible-compressible type so  $\phi$  can be used to chart the phase boundary. Similarly, for the MI phase it transitions to BG, which is a compressible

phase. The DS phase, in the phase diagram, is followed by the SS phase, and we choose  $|S(\pi, \pi)|$  as the order parameter to distinguish these two phases. As the DS phase is a solid phase with rare SF islands, it has higher density contrast and hence, possesses larger value of  $|S(\pi, \pi)|$  than SS. Consequently, we set  $|S(\pi, \pi)| \geq 0.9$  as the threshold in the bisection method to determine the DS-SS phase boundary. On increasing  $J/U$  further, we encounter the SS-SF phase boundary and for the determination of phase boundary between SS and SF, we choose  $|S(\pi, \pi)|$  as the order parameter and we consider  $|S(\pi, \pi)| \geq 10^{-3}$  as the threshold to determine the phase boundary between SS and SF phase.

To determine the effects of long-range interactions we begin by examining the quantum phases of DBHM, in which only the on-site interactions is considered. The phase diagram of the system for  $D/U = 0.2$  is shown in Fig. 2. It shows the existence of BG phase for low  $J \lesssim 0.005U$  in a small region between the incompressible Mott lobes and it also exist as a thin patina surrounding the Mott lobes. The latter is consistent with the theorem of inclusions [22]. According to which in presence of disorder the MI-SF transition is intervened by the BG phase. As expected, the DW phase is absent without the long-range interactions and consequently, the DS phase does not occur in the phase diagram. The quantum phases with diagonal long-range order emerge in the system with the introduction of the long-range interactions, and these are examined in detail.

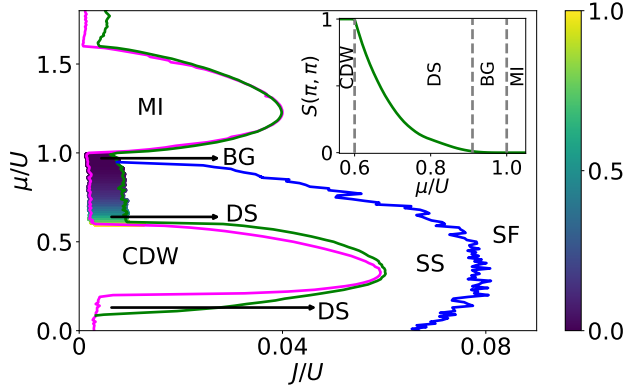


FIG. 5. Ground state phase diagram of DEBHM for  $V_1/U = 0.2$  and  $D/U = 0.2$ . The violet phase boundary indicates the phase boundary between the insulating phases (CDW, MI) and disordered phases (DS, BG). The green phase boundary indicates the phase boundary between disordered phases and supersolid and superfluid. The blue phase boundary indicates the phase boundary between SS and SF. The color gradient between the CDW lobe and MI lobe is plotted based on  $|S(\pi, \pi)|$  and it indicates the transition from DS to BG in between the lobes. The inset shows the plot of the structure factor  $S(\pi, \pi)$  at  $J/U = 0.005$  as a function of the  $\mu/U$ .

### 1. Nearest neighbour interaction

The distinguishing feature of DEBHM is the emergence of the DS phase characterized by zero  $\rho_s$ , but finite  $\phi_{p,q}$  and

$S(\pi, \pi)$ . Using SGMF we first generate ground state phase diagrams of the system by considering NN interaction, that is, only  $V_1$  is non-zero. For  $zV_1 < 1$ , where  $z$  is the co-ordination number, the model has CDW phase or MI phase as the insulating quantum phase of the ground state. In the absence of disorder ( $D/U = 0$ ) the CDW phase undergoes a quantum phase transition to the SS phase when  $J/U$  is increased. The transition is evident from the phase diagram shown in Fig. 3(a). However, as discernible from the phase diagram in Fig. 3(b), the introduction of disorder with  $D/U = 0.05$  leads to the emergence of the DS phase and it intervenes the transition from CDW to SS. This is akin to BG phase intervening the transition from MI to SF when disorder is introduced to BHM. The DS phase is compressible but possesses the character of a solid. The latter is associated with diagonal long-range order and characterized by finite structure factor. The solid lobes shrink further as the strength of the disorder is increased, which is evident from the phase diagram for  $D/U = 0.1$  as shown in Fig. 3(c). However, as noticeable in the figure, the SS phase is enhanced. For illustration, the density distribution for some of the quantum phases, present in the phase diagrams shown in Fig. 3, are shown in Fig. 4.

The presence of the BG phase around the MI lobe is not obvious for  $D/U = 0.1$ . However, as the disorder is increased the existence of the BG phase becomes more prominent. Thus, as shown in Fig. 5, the BG phase surrounding the MI phase is noticeable for  $D/U = 0.2$ . And, similarly, the domain of the DS phase around the CDW lobe is larger compared to  $D/U = 0.1$ . As mentioned earlier,  $\phi$  is used to differentiate the compressible BG phase from the incompressible MI phase. And, the superfluid fraction  $|f_s|$  given in Eq. (14) is used as the order parameter to segregate the BG phase from other compressible phases like SF and SS. We choose  $|f_s| \leq 10^{-7}$  as the threshold to determine the phase boundary between BG and other compressible phases. In contrast to the compressible phases, the incompressible lobes of CDW and MI phases shrink and in between these lobes there is a strip across which DS-BG transition occurs. The transition is indicated by the change in  $|S(\pi, \pi)|$  as we trace it across the strip from lower  $\mu/U$  to higher value for fixed  $J/U$  as shown in the inset of Fig. 5. As seen from the figure, within CDW  $|S(\pi, \pi)|$  is unity and decreases rapidly across the DS, and it is zero in the BG and MI phases. The value of  $|S(\pi, \pi)|$  is zero within BG as it has no diagonal long range order. Thus  $|S(\pi, \pi)|$  becoming zero signals the transition from DS to BG phase. In the MI phase  $|S(\pi, \pi)|$  is zero as it is a uniform density phase. The density and SF order parameter distributions of the quantum phases in this strip are shown in Fig. 6.

To study the effect of disorder on various quantum phases, we increase the disorder strength to  $D/U = 0.3$ , while retaining  $V_1 = 0.2U$ . The resulting phase diagram is shown in Fig. 7(a). The figure shows that MI phase shrinks significantly and survives only in a small region. Notably, the MI phase at larger  $J/U$  is replaced by the BG phase, thereby expanding the BG domain surrounding the MI. The CDW lobe also diminishes, although it continues to occupy a relatively larger area, as its region between the solid lobes expands. In contrast, the SS phase becomes more prominent, now cover-

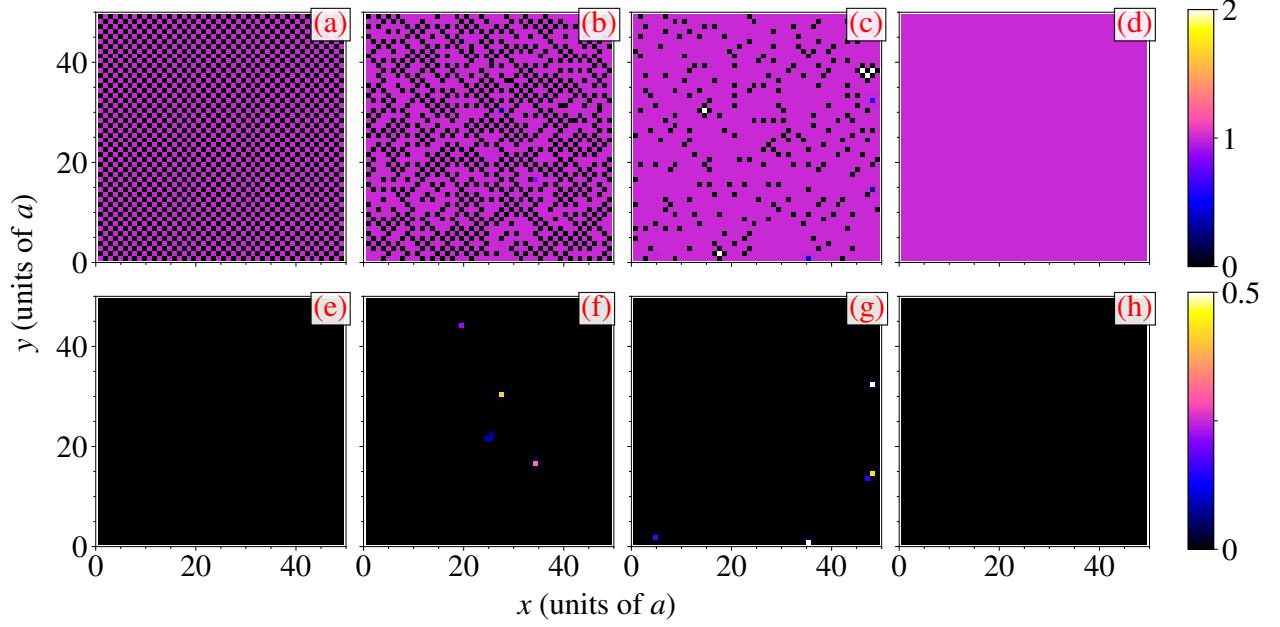


FIG. 6. Boson density and order parameter plots at  $J/U = 0.005, D/U = 0.2$  and  $V_1/U = 0.2$ . Panels (a)-(d) shows the density plots and (e)-(h) shows the SF order parameter plots for  $\mu/U = 0.55, 0.75, 0.96$  and  $1.04$  corresponding to the CDW, DS, BG and MI phases respectively.

ing a larger portion of the phase diagram. Thus the disorder has a larger impact on the MI phase than the CDW phase. And, the SS phase with both diagonal and off-diagonal long-range orders is favored. The sensitivity of MI phase to disorder is due to the ease with which the commensurate filling can be disrupted. In comparison, The CDW phase maintains the diagonal long-range order and incompressibility even under increasing disorder, as its destruction requires rearrangement of particle occupancies across a larger number of lattice sites.

## 2. Nearest and next-nearest neighbour interaction

To examine the impact of the long-range interactions further, we introduce NNN interaction by considering  $V_2 = V_1/(2\sqrt{2})$ . This is the relation when the long-range interaction is of dipole-dipole type having  $1/r^3$  radial dependence. The DEBHM then exhibits four types of insulating quantum phases, these are  $1/4$  DW, CDW,  $3/4$  DW and MI. The phase diagram for the case of  $V_1/U = 0.2$ , which implies  $V_2/U = 0.0707$ , and disorder strength  $D/U = 0.05$  is shown in Fig. 7 (b). In this case,  $|S(\pi, \pi)| \geq 0.45$  is considered as the threshold to determine the phase boundary between DS and SS. From the figure, it is evident that with NNN interaction the SS lobe shrinks. Hence, we can infer that increasing the range of the long-range interaction at fixed disorder strength, promotes SF phase and suppresses the SS phase.

## C. DS-BG transition

To analyse the DS-BG transition which occurs across a vertical strip at  $\mu = 0.91U$  in better detail we examine and compare the trends of various properties. As discussed in the previous section, the DS-BG transition is evident from the phase diagram shown in Fig. 5. One of the important properties is the compressibility  $\kappa$ , and its variation from DS to BG phase for a fixed value of  $J/U$  is shown by the blue curve in Fig. 8(a). In the figure, across the DS domain  $\kappa$  decreases reaching a minima and then, increases sharply on entering the BG domain. This indicates, hardening of the DS phase as it evolves towards the BG phase and reaches a minima before softening. In the DS phase,  $\kappa$  is finite as the disorder modifies  $\mu$  to the effective chemical potential  $\tilde{\mu}$  and which may correspond to the SF or MI phase of the clean eBHM. With the modified  $\mu$ , some of the vacant lattice sites in the CDW can then acquire finite occupancies. The disorder averaged SF order parameter  $\Phi$  is non-zero if some of the vacant lattices acquire fractional occupancies and along the strip the trend of  $\Phi$  is shown by the red curve in Fig. 8(a). Additional vacant sites are filled at higher  $\mu$  and reduces the probability of finding a vacant site. Within the DS phase the occupancy is bounded to unity upto a higher value of  $\mu$  and this limits the possibility to increase the number of particles. As a result, the increase in number of particles in the system slows down with increasing  $\mu$  and  $\kappa$  is expected to decrease. This trend continues till the system enters BG phase at  $\mu \approx 0.91U$ , where few sites with large  $\tilde{\mu}$  host more than unit occupancy leading to a sharp increase in  $\kappa$  and  $\Phi$ .

To check the robustness of the DS-BG phase transition, we examine the transition with the CGMF method. The method



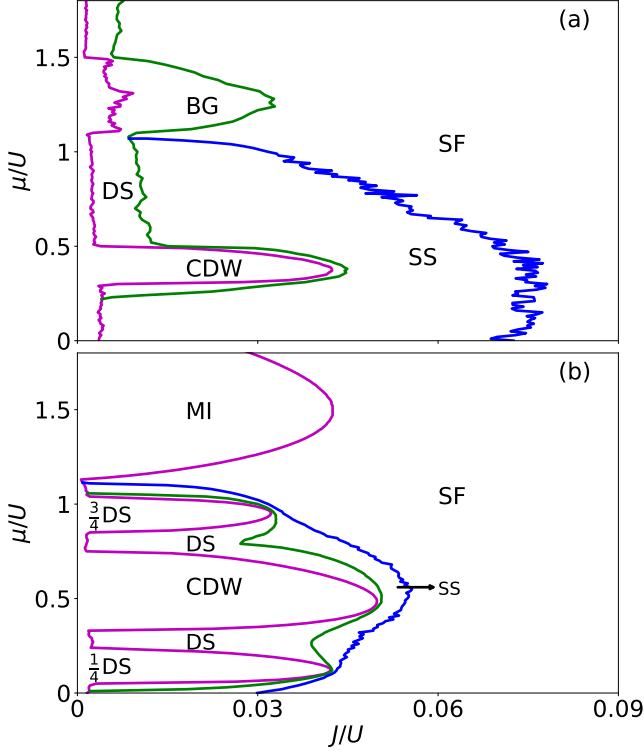


FIG. 7. Panel (a) shows ground state phase diagram of DEBHM for  $V_1/U = 0.2$  and  $D/U = 0.3$  and (b) shows the phase diagram at  $V_1/U = 0.2$ ,  $V_2/U = 0.0707$  and  $D/U = 0.05$ .

incorporates inter-site correlations within a cluster exactly and thus, can provide better description of the phase transition than the SGMF method. The discussions on CGMF method and relevant details, in particular, the numerical considerations are given in previous work [35, 47]. The CGMF results based on cluster size of  $2 \times 2$  suggests that both the DS and BG phases are robust and survives the beyond mean-field effects. With this cluster size and  $N_B = 4$ , the properties of the system as it undergoes DS-BG transition is shown in Fig. 8(b). The trend in  $S(\pi, \pi)$  suggests a transition from the structured DS phase to BG phase at  $\mu \approx 0.89U$ , which is lower than the corresponding SGMF result. The trend in  $\kappa$  and  $\Phi$  also shows, like in the SGMF case, a sharp increase in the BG phase.

The transition from DS to BG is an example of a phase transition which destroys diagonal long-range order and can be studied using tools from percolation theory. In the DS phase, rare island of superfluidity forms on a background of the checkerboard solid. This structured background is eventually destroyed as the system enters the BG phase where the rare SF islands are formed over a MI background. In the BG phase, the MI background comprising of unit occupancy can be seen as a single domain which spans the entire lattice, while in DS solid phase, the domains of unit occupancies are small as evident in Fig. 6(b,c). Thus, the transition of the background phase from checkerboard to MI can be viewed as a percolation of the unit occupancy domains and the span ( $R$ )

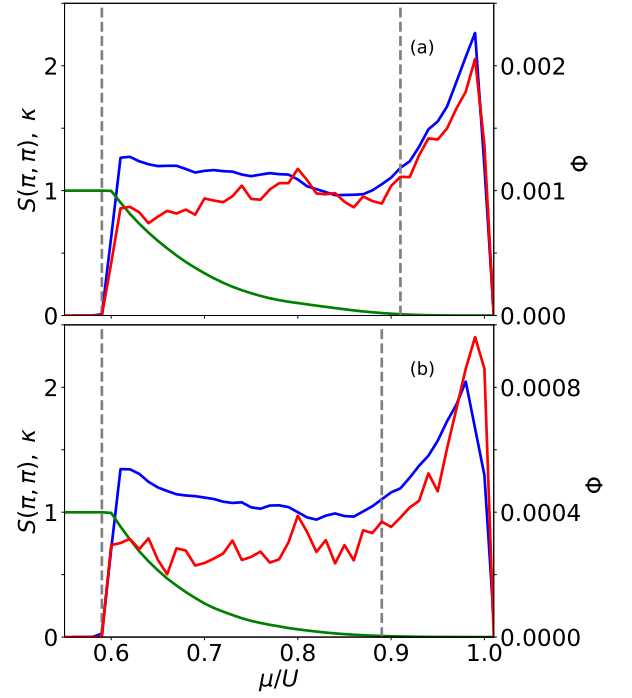


FIG. 8. Panel (a) and (b) displays the disorder averaged properties of the system based on SGMF and CGMF results respectively for  $V_1 = 0.2U$  and  $D = 0.2U$ . Green, blue and red curves represent  $S(\pi, \pi)$ ,  $\kappa$  and  $\Phi$ .

of the largest domain, along the two directions of the lattice would be a property of interest. To identify the domains of unit occupancy and for analysing the span of the largest domains, we use the algorithm discussed in ref. [48]. In Fig. 9, we plot disorder averaged span of the largest domain as a function of  $\mu$ . The figure shows a percolation transition occurring at  $\mu \approx 0.8U$ , which is lower than the DS-BG transition point determined using structure factor with a cut-off  $S(\pi, \pi) = 0.01$ . This is as expected, the percolation analysis determines the onset of the transition from checkerboard to MI phase of the background phase. The percolation transition indicates that there is a large enough domain of MI which extend the entire system along both directions.

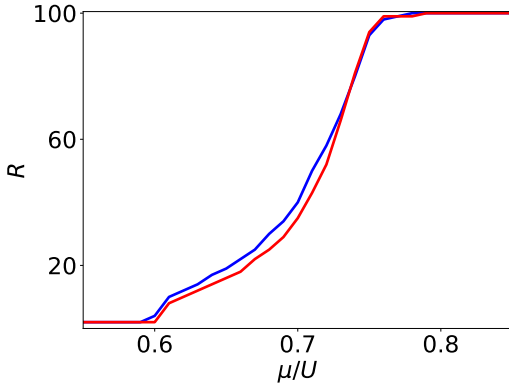


FIG. 9. DS-BG transition as a percolation transition. The span  $R$  of the largest unit occupancy domain is plotted as a function of  $\mu$  for  $V_1 = 0.2$  and  $D = 0.2$ . For a  $50 \times 50$  lattice, spanning domain along the two directions would correspond to  $R = 100$  and this occurs at  $\mu = 0.8U$ . The blue (red) curve are computed using the CGMF (SGMF) results.

## V. CONCLUSIONS

We have examined the zero-temperature quantum phases and quantum phase transitions of soft-core dipolar bosons in a 2D disordered square optical lattice using DEBHM. We

determine the lower energy configuration of bosons in the incompressible or solid phase analytically using the strong-coupling perturbative expansion. We find that the CDW phase is favoured. With the long-range dipolar interactions two types of disordered phases DS and BG emerge. Among these the DS phase has diagonal long-range order. The DS and BG phase emerges when the effective chemical potential (resulting from disorder in lattice potential) allow few of the lattice sites to support superfluidity. At higher disorder  $D/U = 0.2$ , there is a strip adjacent to  $J/U = 0$  along which DS-BG occurs. The robustness of these phases and DS-BG transition is verified using the CGMF method. To understand the DS-BG transition in better detail we have examined various properties of the system using both SGMF and CGMF. The structured CB background phase of the DS undergoes a transition to the homogeneous MI as the system enters BG phase. Thus, the transition of the background phase can be analysed from the perspective of percolation of system by domains of unit occupancy. The percolation results underestimate the transition point, which suggests that the transition should occur after the spanning cluster grows to become the uniform background seen in the MI phase. We also studied the fate of quantum phases at high disorder  $D/U = 0.3$  and observe that the MI lobe shrinks and it is replaced by the BG phase. The CDW lobe, on the other hand, retains the extant of the domain. This indicates that CDW phase is more robust against disorder.

- 
- [1] P. W. Anderson, “Absence of diffusion in certain random lattices,” *Phys. Rev.* **109**, 1492–1505 (1958).
  - [2] Ferdinand Evers and Alexander D. Mirlin, “Anderson transitions,” *Rev. Mod. Phys.* **80**, 1355–1417 (2008).
  - [3] M. P. A. Fisher, P. B. Weichman, G. Grinstein, and D. S. Fisher, “Boson localization and the superfluid-insulator transition,” *Phys. Rev. B* **40**, 546 (1989).
  - [4] L. Fallani, J. E. Lye, V. Guarrera, C. Fort, and M. Inguscio, “Ultracold atoms in a disordered crystal of light: Towards a bose glass,” *Phys. Rev. Lett.* **98**, 130404 (2007).
  - [5] Werner Krauth, Nandini Trivedi, and David Ceperley, “Superfluid-insulator transition in disordered boson systems,” *Phys. Rev. Lett.* **67**, 2307–2310 (1991).
  - [6] V. Gurarie, L. Pollet, N. V. Prokof’ev, B. V. Svistunov, and M. Troyer, “Phase diagram of the disordered bose-hubbard model,” *Phys. Rev. B* **80**, 214519 (2009).
  - [7] B. Deissler, M. Zaccanti, G. Roati, C. D’Errico, M. Fattori, M. Modugno, G. Modugno, and M. Inguscio, “Delocalization of a disordered bosonic system by repulsive interactions,” *Nature Physics* **6**, 354–358 (2010).
  - [8] M. Pasienski, D. McKay, M. White, and B. DeMarco, “A disordered insulator in an optical lattice,” *Nature Physics* **6**, 677–680 (2010).
  - [9] Ji-Ming Gao, Rong-An Tang, and Ju-Kui Xue, “Phase diagram of disordered two-dimensional extended bose-hubbard model,” *Europhysics Letters* **117**, 60007 (2017).
  - [10] Fei Lin, Erik S. Sørensen, and D. M. Ceperley, “Superfluid-insulator transition in the disordered two-dimensional bose-hubbard model,” *Phys. Rev. B* **84**, 094507 (2011).
  - [11] Chiara D’Errico, Eleonora Lucioni, Luca Tanzi, Lorenzo Gori, Guillaume Roux, Ian P. McCulloch, Thierry Giamarchi, Massimo Inguscio, and Giovanni Modugno, “Observation of a disordered bosonic insulator from weak to strong interactions,” *Phys. Rev. Lett.* **113**, 095301 (2014).
  - [12] Sukla Pal, Rukmani Bai, Soumik Bandyopadhyay, K. Suthar, and D. Angom, “Enhancement of the bose glass phase in the presence of an artificial gauge field,” *Phys. Rev. A* **99**, 053610 (2019).
  - [13] M. White, M. Pasienski, D. McKay, S. Q. Zhou, D. Ceperley, and B. DeMarco, “Strongly interacting bosons in a disordered optical lattice,” *Phys. Rev. Lett.* **102**, 055301 (2009).
  - [14] P. Bouyer, “Quantum gases and optical speckle: a new tool to simulate disordered quantum systems,” *Reports on Progress in Physics* **73**, 062401 (2010).
  - [15] Immanuel Bloch, “Ultracold atoms in optical lattices,” *Phys. Rev. Lett.* **95**, 260401 (2005).
  - [16] Oliver Morsch and Markus Oberthaler, “Dynamics of bose-einstein condensates in optical lattices,” *Rev. Mod. Phys.* **78**, 179–215 (2006).
  - [17] M. Lewenstein, A. Sanpera, V. Ahufinger, B. Damski, A. Sen(De), and U. Sen, “Ultracold atomic gases in optical lattices: mimicking condensed matter physics and beyond,” *Adv. Phys.* **56**, 243 (2007).
  - [18] Konstantin V. Krutitsky, “Ultracold bosons with short-range interaction in regular optical lattices,” *Physics Reports* **607**, 1–101 (2016), ultracold bosons with short-range interaction in regular optical lattices.
  - [19] Florian Schäfer, Takeshi Fukuhara, Seiji Sugawa, Yosuke Takasu, and Yoshiro Takahashi, “Tools for quantum simula-

- tion with ultracold atoms in optical lattices,” *Nature Reviews Physics* **2**, 411–425 (2020).
- [20] D. Jaksch, C. Bruder, J. I. Cirac, C. W. Gardiner, and P. Zoller, “Cold bosonic atoms in optical lattices,” *Phys. Rev. Lett.* **81**, 3108 (1998).
- [21] M. Greiner, O. Mandel, T. Esslinger, T. W. Hänsch, and I. Bloch, “Quantum phase transition from a superfluid to a Mott insulator in a gas of ultracold atoms,” *Nature (London)* **415**, 39 (2002).
- [22] L. Pollet, N. V. Prokof’ev, B. V. Svistunov, and M. Troyer, “Absence of a direct superfluid to mott insulator transition in disordered bose systems,” *Phys. Rev. Lett.* **103**, 140402 (2009).
- [23] Massimo Boninsegni and Nikolay V. Prokof’ev, “Colloquium: Supersolids: What and where are they?” *Rev. Mod. Phys.* **84**, 759–776 (2012).
- [24] C. Trefzger, C. Menotti, and M. Lewenstein, “Ultracold dipolar gas in an optical lattice: The fate of metastable states,” *Phys. Rev. A* **78**, 043604 (2008).
- [25] Davide Rossini and Rosario Fazio, “Phase diagram of the extended bose–hubbard model,” *New Journal of Physics* **14**, 065012 (2012).
- [26] Daisuke Yamamoto, Akiko Masaki, and Ippei Danshita, “Quantum phases of hardcore bosons with long-range interactions on a square lattice,” *Phys. Rev. B* **86**, 054516 (2012).
- [27] K. Suthar, Hrushikesh Sable, Rukmani Bai, Soumik Bandyopadhyay, Sukla Pal, and D. Angom, “Supersolid phase of the extended bose-hubbard model with an artificial gauge field,” *Phys. Rev. A* **102**, 013320 (2020).
- [28] Andrea Morales, Philip Zupancic, Tilman Esslinger, and Tobias Donner, “Supersolid formation in a quantum gas breaking a continuous translational symmetry,” *Nature* **543**, 87–90 (2017).
- [29] L. Tanzi, E. Lucioni, F. Famà, J. Catani, A. Fioretti, C. Gabbanini, R. N. Bisset, L. Santos, and G. Modugno, “Observation of a dipolar quantum gas with metastable supersolid properties,” *Phys. Rev. Lett.* **122**, 130405 (2019).
- [30] Fabian Böttcher, Jan-Niklas Schmidt, Matthias Wenzel, Jens Hertkorn, Mingyang Guo, Tim Langen, and Tilman Pfau, “Transient supersolid properties in an array of dipolar quantum droplets,” *Phys. Rev. X* **9**, 011051 (2019).
- [31] L. Chomaz, D. Petter, P. Ilzhöfer, G. Natale, A. Trautmann, C. Politi, G. Durastante, R. M. W. van Bijnen, A. Patscheider, M. Sohmen, M. J. Mark, and F. Ferlaino, “Long-lived and transient supersolid behaviors in dipolar quantum gases,” *Phys. Rev. X* **9**, 021012 (2019).
- [32] D. S. Rokhsar and B. G. Kotliar, “Gutzwiller projection for bosons,” *Phys. Rev. B* **44**, 10328 (1991).
- [33] K. Sheshadri, H. R. Krishnamurthy, R. Pandit, and T. V. Ramakrishnan, “Superfluid and insulating phases in an interacting-boson model: Mean-field theory and the RPA,” *EPL* **22**, 257 (1993).
- [34] Chao Zhang and Heiko Rieger, “The effect of disorder on the phase diagrams of hard-core lattice bosons with cavity-mediated long-range and nearest-neighbor interactions,” *Frontiers in Physics* **7** (2020), 10.3389/fphy.2019.00236.
- [35] Dirk-Sören Lühmann, “Cluster gutzwiller method for bosonic lattice systems,” *Phys. Rev. A* **87**, 043619 (2013).
- [36] S. R. Broadbent and J. M. Hammersley, “Percolation processes: I. crystals and mazes,” *Mathematical Proceedings of the Cambridge Philosophical Society* **53**, 629–641 (1957).
- [37] P. J. Flory, *Principles of polymer chemistry* (Cornell university press, 1953).
- [38] R. J. Elliott, B. R. Heap, D. J. Morgan, and G. S. Rushbrooke, “Equivalence of the critical concentrations in the ising and heisenberg models of ferromagnetism,” *Phys. Rev. Lett.* **5**, 366–367 (1960).
- [39] D. Stauffer and A. Aharony, *Introduction To Percolation Theory* (1992).
- [40] Soumik Bandyopadhyay, Rukmani Bai, Sukla Pal, K. Suthar, Rejish Nath, and D. Angom, “Quantum phases of canted dipolar bosons in a two-dimensional square optical lattice,” *Phys. Rev. A* **100**, 053623 (2019).
- [41] Rukmani Bai, Deepak Gaur, Hrushikesh Sable, Soumik Bandyopadhyay, K. Suthar, and D. Angom, “Segregated quantum phases of dipolar bosonic mixtures in two-dimensional optical lattices,” *Phys. Rev. A* **102**, 043309 (2020).
- [42] R. Roth and K. Burnett, “Superfluidity and interference pattern of ultracold bosons in optical lattices,” *Phys. Rev. A* **67**, 031602 (2003).
- [43] M. Iskin and J. K. Freericks, “Strong-coupling perturbation theory for the extended bose-hubbard model,” *Phys. Rev. A* **79**, 053634 (2009).
- [44] Rashi Sachdeva and Sankalpa Ghosh, “Density-wave–supersolid and mott-insulator–superfluid transitions in the presence of an artificial gauge field: A strong-coupling perturbation approach,” *Phys. Rev. A* **85**, 013642 (2012).
- [45] J. K. Freericks and H. Monien, “Strong-coupling expansions for the pure and disordered bose-hubbard model,” *Phys. Rev. B* **53**, 2691–2700 (1996).
- [46] Tao Wang, Xue-Feng Zhang, Chun-Feng Hou, Sebastian Eggert, and Axel Pelster, “High-order symbolic strong-coupling expansion for the bose-hubbard model,” *Phys. Rev. B* **98**, 245107 (2018).
- [47] Rukmani Bai, Soumik Bandyopadhyay, Sukla Pal, K. Suthar, and D. Angom, “Bosonic quantum hall states in single-layer two-dimensional optical lattices,” *Phys. Rev. A* **98**, 023606 (2018).
- [48] Hrushikesh Sable, Deepak Gaur, and D. Angom, “Fine-grained domain counting and percolation analysis in two-dimensional lattice systems with linked lists,” *Phys. Rev. E* **108**, 045307 (2023).